Agricultural and Forest Meteorology 378 (2026) 110966

Contents lists available at ScienceDirect

Agricultural and Forest Meteorology

journal homepage: www.elsevier.com/locate/agrformet

Tracking canopy conductance and transpiration of CAM-plants *Agave sisalana* with carbonyl sulfide fluxes

Kukka-Maaria Kohonen [a,b,*], Angelika Kübert [b], Lutz Merbold [c,d], Matti Räsänen [e], Nina Buchmann [a], Ivan Mammarella [b], Petri Pellikka [f,g,h], Timo Vesala [b,e]

[a] Department of Environmental Systems Science, ETH Zurich, Zurich, 8092, Switzerland
[b] Institute for Atmospheric and Earth System Research/Physics, Faculty of Science, University of Helsinki, P.O. Box 68, Helsinki, 00014, Finland
[c] Integrative Agroecology Group, Research Division for Agroecology and Environment, Agroscope, Reckenholzstrasse 191, Zurich, 8046, Switzerland
[d] Mazingira Centre, International Livestock Research Institute, Old Naivasha Road, Nairobi, 00100, Kenya
[e] Institute for Atmospheric and Earth System Research/Forest Sciences, Faculty of Agriculture and Forestry, University of Helsinki, Helsinki, 00014, Finland
[f] Department of Geosciences and Geography, University of Helsinki, P.O. Box 64, Helsinki, 00014, Finland
[g] State Key Laboratory of Information Engineering and Surveying, Mapping and Remote Sensing, Wuhan University, Wuhan, PR China
[h] Finnish Southern Africa Cooperation Institute (FSAI), 10 Schwabe Street, Windhoek, Namibia

ARTICLE INFO

Dataset link: https://doi.org/10.5281/zenodo.17855873, https://doi.org/10.5281/zenodo.14445518

Keywords:
CAM
Eddy covariance
COS
Stomatal conductance
Transpiration
Flux measurements
Ecosystem scale

ABSTRACT

Crassulacean acid metabolism (CAM) helps plants in arid regions to reduce water loss by opening their stomata and taking up carbon dioxide (CO_2) during nighttime. While gas exchange in CAM plants has been mainly studied under controlled laboratory conditions, only a few ecosystem scale studies exist. Moreover, carbonyl sulfide (COS) has been used as a tracer for stomatal conductance, transpiration and photosynthesis in C_3 and C_4 plants, but no studies on CAM ecosystems have yet been published. Here we present the first ecosystem scale measurements of COS fluxes over *Agave sisalana* (CAM plant), commercially cultivated for its fiber. The measurements were made during the wet season in Kenya. The ecosystem was a consistent sink of COS, with higher uptake observed during nighttime (−11.5 pmol m^{-2} s^{-1}) than during daytime (-5.6 pmol m^{-2} s^{-1}). The magnitude of COS fluxes was comparable to non-growing season daytime fluxes reported for C_3 and C_4 plant dominated ecosystems. The soil was a small COS source (0.3 pmol m^{-2} s^{-1}), with highest emissions under high radiation and temperature conditions. Using random forest modeling, we found that vapor pressure deficit, air temperature and soil water content were the most important drivers of nighttime ecosystem COS exchange (variable importance 0.25, 0.23 and 0.20, respectively), indicating the importance of stomatal limitation for COS fluxes. During daytime, air temperature, photosynthetically active radiation and soil temperature were the most important drivers (variable importances 0.19, 0.18 and 0.18, respectively). COS fluxes were further used to track canopy stomatal conductance and transpiration and compared to another transpiration estimate from the conditional eddy covariance method, which is based on raw water vapor and vertical wind data from eddy covariance. Conductance values ranged from 0.03 ± 0.06 mol m^{-2} s^{-1} during daytime to 0.06 ± 0.02 mol m^{-2} s^{-1} during nighttime. Transpiration was thus higher during nighttime than during daytime, reflecting the CAM gas exchange strategy.

1. Introduction

Plants with crassulacean acid metabolism (CAM) are well adapted to reduce water loss in arid environments by keeping their stomata closed during the day but opening them at night for carbon dioxide (CO_2) uptake. Because of this pronounced diel pattern, water use efficiency (*WUE*) of CAM plants can be three times higher than that of C_4 plants and six times higher than that of C_3 plants (Borland et al., 2009). In addition, the annual water demand of CAM plants is only one-quarter that of C_4 plants and one-sixth that of C_3 plants, making them highly drought tolerant (Borland et al., 2009; Yang et al., 2015). However, their biomass production is often lower than that of C_3 plants (Lüttge, 2004), although some *Agave* and *Opuntia* species have been found to reach similar or even higher productivity compared to C_3 plants (Nobel, 1996).

The diel CAM gas exchange cycle consists of four phases as defined by Osmond (1978). During the night (phase I), CAM plants take up

* Corresponding author at: Department of Environmental Systems Science, ETH Zurich, Zurich, 8092, Switzerland.
E-mail address: kukkamaaria.kohonen@usys.ethz.ch (K.-M. Kohonen).

https://doi.org/10.1016/j.agrformet.2025.110966
Received 5 June 2025; Received in revised form 21 September 2025; Accepted 27 November 2025
Available online 10 December 2025

CO_2, along with other gases, from the atmosphere. CO_2 is bound to malic acid by the enzyme phosphoenolpyruvate carboxylase (PEPC) and stored until light becomes available during the day. Then CO_2 is regenerated from malic acid and fixed by the enzyme ribulose-1,5-bisphosphate carboxylase/oxygenase (RuBisCO) (phase III; Cushman (2001)). Phases II and IV of the CAM gas exchange cycle are the transient phases in the early morning and late afternoon, respectively, when CO_2 can also be assimilated directly in the Calvin cycle (Griffiths et al., 2007).

Globally, CAM plants are estimated to make up over 6% of vascular plant species (Winter and Smith, 1996), but in arid regions, they can occupy up to 25% of the vegetative surface (Osmond, 1978). Currently, plants with CAM photosynthesis are not included in land surface models such as SiB4 (Kooijmans et al., 2021) or ORCHIDEE (Maignan et al., 2021), which only include plants with C_3 or C_4 photosynthesis. Although their global importance is limited, CAM plants may play a significant role in drylands which cover about 41% of Earth's terrestrial surface (Millennium ecosystem assessment, 2005). Thus, while CAM plants might control regional carbon budgets, our knowledge of flux magnitudes of CAM-dominated ecosystems is scarce.

One reason for their exclusion from land surface models is the lack of gas exchange measurements of CAM plants under field conditions. In the laboratory, gas exchange patterns of CAM plants have been measured, and the expected reverse diel pattern of CO_2 exchange compared to C_3 and C_4 plants has been found (Nobel and Valenzuela, 1987; Winter, 2019). Eddy covariance (EC) CO_2 flux measurements have been performed on tequila (*Agave tequilana*) (Owen et al., 2016), *Opuntia stricta* cactus (Jardim et al., 2023), pineapple (*Ananas comosus*) (San-José et al., 2007) and sisal (*Agave sisalana*) (Skogberg et al., 2025). *Agave tequilana* (Owen et al., 2016), *Ananas comosus* (San-José et al., 2007) and *Agave sisalana* (Skogberg et al., 2025) showed the typical CAM diel cycle with nighttime CO_2 uptake and daytime release or near-zero fluxes, whereas *Opuntia stricta* cactus (Jardim et al., 2023) only showed daytime CO_2 uptake. Moreover, Skogberg et al. (2025) found that the daytime CO_2 emission was greater during a dry season than during a wet season, while nighttime CO_2 uptake stayed at the same level of magnitude through both seasons. Previous studies on CAM ecosystems have found that the cumulative amount of radiation as well as temperature and vapor pressure deficit (*VPD*) during the day affected the CO_2 uptake of the following night (Owen et al., 2016). In addition, cold nights have been found to increase the nocturnal CO_2 uptake (Owen et al., 2016). However, previous ecosystem scale studies have focused solely on net ecosystem CO_2 exchange (*NEE*) and have not pursued partitioning *NEE* into respiration and gross primary production (*GPP*). Traditional *NEE* partitioning methods (Reichstein et al., 2005; Lasslop et al., 2010) cannot be directly implemented to CAM plants due to the reversed diel cycle compared to C_4 and C_3 plants as well as functional plasticity with non-CAM behavior. Moreover, nighttime CO_2 uptake does not necessarily equate to *GPP*, as not all carbon stored during the night may be used for photosynthesis during the next day. Hence, other approaches need to be employed for partitioning *NEE* fluxes of CAM ecosystems.

Evapotranspiration (*ET*) is closely coupled with the CO_2 cycle through stomata, and this coupling is described by *WUE* (Keenan et al., 2013). In land surface models, *WUE* serves both as a diagnostic and a mechanistic constraint. It provides a method to evaluate and parameterize stomatal control on carbon uptake and water loss, and serves as a scaling parameter across leaf, ecosystem, and global scales. *WUE* can be estimated from *GPP* and transpiration (*T*) as $WUE = GPP/T$, when it describes the photosynthetic carbon fixation and plant water loss (Stoy et al., 2019). Some studies, on the other hand, calculate *WUE* as $WUE_{NET} = NEE/ET$, which provides a measure of the overall ecosystem carbon balance in relation to ecosystem water loss (Owen et al., 2016). *ET* can be calculated from the water vapor (H_2O) fluxes measured by the EC method. However, partitioning *ET* into its components, evaporation (*E*) and transpiration, is challenging at ecosystem scale but important for the further improvement of land surface models (Stoy et al., 2019). A new development for *ET* partitioning was introduced by Zahn et al. (2022). This partitioning method, called conditional eddy covariance (CEC), uses raw EC data and distinguishes time periods when the fluctuation of both CO_2 and H_2O is positive (net emission), indicating soil respiration and *E*, while a negative fluctuation of CO_2 (net uptake) simultaneously with a positive H_2O fluctuation indicates photosynthesis and *T*. However, this method has not yet been widely applied or tested for terrestrial ecosystems, including CAM ecosystems.

Carbonyl sulfide (COS) has attracted attention lately because it can be used as a proxy for stomatal conductance and thus for (gross) photosynthesis (Sandoval-Soto et al., 2005; Asaf et al., 2013), and transpiration (Wehr et al., 2017; Berkelhammer et al., 2020). COS is taken up by plants through stomata like CO_2, until it reaches the chloroplast surface, where it is consumed in a hydrolysis reaction using the enzymes carbonic anhydrase (CA) and PEPC (Protoschill-Krebs and Kesselmeier, 1992; Wohlfahrt et al., 2012). To our knowledge, there are currently no studies focusing on the COS biochemistry of CAM plants. Since CA and PEPC are available in CAM plants similar to C_3 plants, the hydrolysis process is assumed to be similar. Complications of using COS as a proxy for *GPP* at ecosystem scale include unknown sinks and sources in the soil (Maseyk et al., 2014; Spielmann et al., 2020), the measurement precision of COS fluxes (Kohonen et al., 2020), and the uncertainty in estimating the leaf relative uptake (*LRU*), i.e., the ratio of COS and CO_2 uptake at leaf scale (Kooijmans et al., 2019; Yang et al., 2018; Sun et al., 2018; Kohonen et al., 2022). However, to date, field studies have mainly focused on C_3 (Asaf et al., 2013; Spielmann et al., 2019; Wehr et al., 2017; Vesala et al., 2022) and C_4 (Berkelhammer et al., 2020) plant-dominated ecosystems, and no COS flux measurements over CAM ecosystems have been published.

In this study, we measured COS fluxes using the EC technique (Aubinet et al., 2012) over a sisal (*Agave sisalana*) plantation in Kenya. The measurement period covered four weeks during the wet season in November–December 2019 and included 12 days of soil chamber flux measurements. Our aims were to (1) track the diel pattern of the CAM COS gas exchange, (2) identify its main environmental drivers, (3) quantify the canopy stomatal conductance of sisal using COS together with H_2O flux measurements, (4) partition *ET* into its *E* and *T* components using the ecosystem scale COS, CO_2 and H_2O flux measurements, and finally (5) calculate the *WUE* and WUE_{NET} of sisal. We hypothesize that COS fluxes follow the same diurnal pattern as CO_2 fluxes with uptake observed at night and can be used to track stomatal conductance of CAM plants.

2. Materials and methods

2.1. Site description

The measurements were carried out at an *Agave sisalana* Perrine plantation, Teita estate, in Mwatate in Taita-Taveta county, Kenya (3°32' S, 38°24'E, 844 m asl) (Fig. S1). Sisal is cultivated for its fiber, traditionally used in making, e.g., ropes, carpets and baskets. In the recent years, sisal has gained more attention as a productive and durable natural fiber with high commercial value (Kozłowski et al., 2020). From Teita estate, most of the fiber is transported overseas for production. The plantation covers an area of 129.5 km^2, making it one of the largest in the world (Wachiye et al., 2021). Sisal has various growth stages, from recently planted up to 20 years old blocks. Sisal is planted in double rows with 0.9 m distance between the plants and 2–3 m distance between the rows. Sisal waste is applied as fertilizer at the time of planting, but no further fertilization is applied afterwards (Wachiye et al., 2021). According to Vuorinne et al. (2021a,b), the biomass densities in the estate ranged from 0 to 46.7 Mg ha^{-1}, depending on the age of the plants (mean biomass 10.6 Mg ha^{-1}). The flux measurements were made within a 2.6 ha field block growing sisal as a pure culture with spontaneous weeds coming

in. The field block had a gentle 5° slope facing the east. Sisal plants were mature, 5 years old and approximately 1.1 m high (Skogberg et al., 2025). The estate has a yearly average temperature of 24 °C and annual rainfall of approximately 600 mm. The soils are latosols, with low soil organic carbon content of around 1% (Pellikka et al., 2023). The area is characterized by dry as well as wet seasons, with a long wet season from March to May, followed by a long dry season from June until October, a short wet season from November to December, and a short dry season until February. The COS flux measurements were carried out during the short wet season from 23 November 2019 until 21 December 2019 (referred to as wet season in the following), while CO_2 flux, and meteorological measurements extended to the dry season until 26 January 2020. Herbicide was sprayed five days prior to the start of the measurements to prevent weeds with C_3 or C_4 photosynthesis growing in the EC footprint area. CO_2 fluxes from the same measurement campaign are reported in Skogberg et al. (2025).

The times presented in this study are in local time (UTC+3), and nighttime is defined when photosynthetically active radiation *PAR* < 10 μmol m^{-2} s^{-1}. Negative fluxes depict uptake by the ecosystem, while positive fluxes depict emissions.

2.2. Meteorological measurements

Air temperature (T_{air}) and relative humidity (*RH*) (Rotronic Instrument Corp., NY, USA) and *PAR* (LI-190R quantum sensor, LI-COR Inc., Nebraska, USA) were measured at 1.5 m above ground, approximately 0.5 m above the sisal leaves. Soil temperature (T_{soil}; Pt100 thermocouples) was measured at two locations; one shaded by sisal and one without shading, both buried in topsoil at 2 cm depth. Soil water content (*SWC*; Theta Probe ML3, Delta-T Devices, Cambridge, UK) was measured in the topsoil (0–5 cm) close to the sisal plant, to represent the water supply for the sisal rooting system, with one sensor. All measurements were logged every minute and averaged every 30 min. Precipitation was measured with a tipping bucket rain gauge (Campbell ARG100, Campbell Scientific, Logan, Utah, USA) from 30 November 2019 onwards and logged every hour. Precipitation measurements 23–30 November 2019 were taken as an average of two nearby weather stations in Maktau (run by University of Helsinki, approximately 30 km to the West) and Voi (run by Kenya Meteorological Department, approximately 30 km to the East), that were found to follow similar precipitation pattern during the time of overlapped measurements.

2.3. Eddy covariance measurements and processing

EC measurements were done at 2.6 m height using an ultrasonic anemometer (USA-1, Metek GmbH, Elmshorn, Germany) for measuring horizontal and vertical wind speeds (Fig. S1 a). COS, CO_2 and H_2O mixing ratios were measured with a quantum cascade laser spectroscopy analyser (QCLS, Aerodyne Research Inc., Billerica, MA, USA). Additionally, CO_2 and H_2O mixing ratios were measured with an infrared gas analyzer (IRGA, LI-7200, LI-COR Inc., Nebraska, USA). Inlet lines were 7 and 0.7 m long for the QCLS and IRGA, respectively, and the inner diameters were 4 mm. The inlet lines were heated to prevent water condensation in the tubing. All measurements were recorded at 10 Hz frequency. The QCLS was calibrated before the measurement campaign using a calibration cylinder with known COS and CO_2 concentrations (Kohonen et al., 2020). Half-hourly background measurements with high-purity nitrogen (N_2) were performed from 25 November until 28 November to remove background spectral structures in the QCLS (Kooijmans et al., 2016). The mean mixing ratio of COS during this time was 394 ppt (Fig. S2), which was later used in conductance and ecosystem relative uptake (*ERU*) calculations. The fluxes were processed using EddyUH software (Mammarella et al., 2016), which is customized for COS flux calculation, following the recommendations given in Kohonen et al. (2020). Time lags between the signals from the sonic anemometer and the gas analyzers were determined with the covariance maximization method. Since the signal-to-noise ratio of COS is low, time lag of CO_2 from the QCLS was used also for COS (Kohonen et al., 2020). The processing included linear detrending, 2D coordinate rotation, despiking data (limits for subsequent datapoints being 50 ppm, 5 ppb and 10 mmol mol^{-1} for CO_2, COS and H_2O, respectively) and spectral corrections for both low (Rannik, 1998) and high frequency (Aubinet et al., 2000) spectral losses. The limit of detection, estimated as suggested in Langford et al. (2015), was 5.8 pmol m^{-2} s^{-1} for COS, 0.055 μmol m^{-2} s^{-1} for CO_2, and 0.0079 mmol m^{-2} s^{-1} for H_2O fluxes, on average. Friction velocity (u_*) filtering was applied to remove periods with low atmospheric turbulence when $u_* < 0.12$ m s^{-1} (Aubinet et al., 2000; Skogberg et al., 2025). Quality screening was applied so that maximum number of allowed spikes in each 30 min period was 100 and the second wind rotation angle was less than 10°. After all quality screening and filtering, 50% (53% nighttime and 46% daytime) of COS and 79% (69% nighttime and 86% daytime) of CO_2 fluxes were left for analysis. The flux footprint covered only the sisal plantation (Fig. S1b; footprint calculation after Kljun et al. (2015)).

ERU was calculated as the ratio of COS to CO_2 deposition velocities as in Asaf et al. (2013)

$$ERU = \frac{FCOS}{FCO2}\frac{\chi_{CO2,a}}{\chi_{COS,a}} \quad (1)$$

where *FCOS* and *FCO2* are the ecosystem scale COS and CO_2 fluxes, and $\chi_{COS,a}$ (kept as a constant value 394 ppt, as described above) and $\chi_{CO2,a}$ (from LI-7200 measurements) are the atmospheric COS and CO_2 mixing ratios, respectively.

2.4. Driver analysis and gap-filling

The most important drivers of the fluxes were found and fluxes gap-filled using a model created with random forest (RF; *RandomForestRegressor* from Python package *sklearn*). The models were trained using a randomly selected subset of the dataset (70%), the variables used as model features (i.e., drivers) were CO_2 flux (for gap-filling COS and H_2O fluxes only), H_2O flux (for gap-filling COS and CO_2 fluxes), air and soil temperatures, *VPD*, *PAR* and *SWC*. The model hyperparameters used were n_estimators=50, max_features=1.0, and random_state=44. The resulting models were validated against the test data set (coefficient of determination R^2=0.62 and root mean square error RMSE=10.6 pmol m^{-2} s^{-1} for COS fluxes; R^2=0.94 and RMSE=1.12 μmol m^{-2} s^{-1} for CO_2 fluxes; R^2=0.95 and RMSE=0.396 mmol m^{-2} s^{-1} for H_2O fluxes).

To better interpret the RF model output, we used SHapley Additive exPlanations (SHAP) analysis, based on principles of game theory (Shapley, 1953). SHAP analysis (Python function *TreeExplainer* from package *shap*) was done to study the contribution of each environmental driver (i.e., feature) to the model output (i.e., the modeled response variable), as well as to identify the temporal variation of the driver importance in more detail. The effect of each driver is given as so-called SHAP value in the unit of the response variable: positive SHAP values represent a positive effect of the driver on the response variable (thus increasing the predicted response variable), while negative SHAP values represent a negative effect of the driver on the response variable (thus decreasing the predicted response variable), always relative to the overall mean of the predicted response variable. The RF model prediction at any given time point is the sum of all feature SHAP values and the average prediction. Thus, all SHAP values are in the unit of the response variable. Only measured data were used for model training and driver analysis, while gap-filled flux data were only used in time series visualizations.

Since CAM plants fix CO_2 into malic acid at nighttime, releasing it for actual photosynthetic CO_2 fixation during daytime (gross primary production, *GPP*), we defined another variable to describe the amount of CO_2 fixed by the sisal plants during the night to be later used in daytime photosynthesis, i.e., the gross primary uptake (*GPU*). Ecosystem CO_2 fluxes were partitioned into *GPU* and respiration using the

LI-7200 flux measurements from the (short) dry season, defined here as from 21 Dec 2019 to 26 Jan 2020 (Skogberg et al., 2025). The dry season daytime CO_2 flux was assumed to consist only of respiration in the lack of daytime C_3 photosynthesis (Skogberg et al., 2025) and was used as input to train a RF model for ecosystem respiration (R_{eco}). The model was then applied for the whole dataset to model R_{eco} and finally to calculate gross primary uptake as $GPU = R_{eco}$ - NEE. Based on this partitioning, we calculated sisal $WUE = GPU/T$. To better compare WUE with earlier studies, we also calculated an ecosystem scale $WUE_{NET} = NEE/ET$.

2.5. Chamber measurements and flux calculation

Chamber measurements were carried out at three different soil cover types: one with bare soil, one with non-CAM weeds growing on soil, and one with grass and old sisal roots on top of the soil (Fig. S1 c-e). One chamber head (height 40 cm, diameter 31.3 cm) was rotated for use on each soil cover type for both ambient light and darkened conditions. Stainless-steel chamber collars were installed one day before the first chamber measurement and left in place during the whole measurement campaign. The chamber head used in the study was cylindrical, made of acrylic plastic, and had a volume of 31 L (Fig. S1 f). The chamber head had a small fan inside to mix the air, and air temperature inside the chamber was measured. The chamber was sealed by pouring bottled water into the groove of the collar, where the chamber head was placed (Korrensalo et al., 2018). Polytetrafluoroethylene (PTFE) tubing of 1/8" diameter was connected from the chamber to the QCLS for COS, CO_2 and H_2O mixing ratio measurements. Another 50 cm long copper tubing with 2 mm inner diameter was added from the chamber to open air to allow pressure equilibration inside the chamber (Heinemeyer and McNamara, 2011). The sampling flow was set to 0.3 LPM, and each chamber was closed for 5 min. After closure at ambient light conditions, the chamber was flushed and covered for a darkened closure. For blank measurements (to ensure no emission or sink from the chamber itself), the collars were covered with PTFE foil and chamber measurements repeated as described above. The blank measurements showed no emissions of COS from the chamber.

Chamber fluxes (F_{ch}) were calculated from the slope of the linear fit made to the concentration data ($\frac{d\chi}{dt}$) collected during the first 3 min (for COS and CO_2) or 1 min (for H_2O) of the chamber closure, before the concentration change was saturated:

$$F_{ch} = \frac{d\chi}{dt}\frac{P_a V}{RTA}. \quad (2)$$

Air pressure (P_a) was assumed to be the normal atmospheric pressure 101 325 Pa, universal gas constant R = 8.31446 J mol K^{-1}, chamber volume V = 0.031 m^3, T the average air temperature measured inside the chamber during closure (in K) and chamber surface area A = 0.077 m^2. The measurements were omitted if the normalized RMSE of the fit was more than 0.3 or if $R^2 < 0.8$. Number of chamber flux measurements left after quality screening were 22, 23, and 21 out of 24 measurements taken in total for the bare soil, weed covered and sisal root covered soil cover types, respectively.

2.6. Canopy conductance and ET partitioning

Canopy conductance for COS was calculated from $FCOS$ according to Wohlfahrt et al. (2012) ($g_{c,COS,COS}$):

$$g_{c,COS,COS} = \frac{-FCOS}{\chi_{COS,a} - \chi_{COS,i}} \quad (3)$$

where $\chi_{COS,a}$ and $\chi_{COS,i}$ are the dry mixing ratios of COS in the atmosphere and in the intercellular spaces, respectively. Assuming boundary layer and mesophyll conductances to be high (Kooijmans et al., 2019; Sun et al., 2024; Wehr et al., 2017), negligible soil fluxes, a very small $\chi_{COS,i}$, and a factor of 1.94 to account for the difference between COS and H_2O conductances due to different molecular diffusivities (Seibt et al., 2010; Stimler et al., 2010), Eq. (3) reduces to give the canopy conductance for H_2O (g_c)

$$g_{c,COS} = \frac{-1.94FCOS}{\chi_{COS,a}} \quad (4)$$

Additionally, for comparison, canopy conductance was also calculated from ecosystem latent heat fluxes (LE) according to Wehr and Saleska (2021) ($g_{c,ET}$). In this method, both LE and sensible heat fluxes (H) were used together with the flux–gradient equations to determine canopy conductance. This method is less prone to biases than the widely used inversed Penman-Monteith equation (Monteith, 1965; Grace et al., 1995) due to the use of measured H. However, like the inversed Penman-Monteith equation, this method works properly only when evaporation can be assumed negligible. Without proper ET partitioning, it is impossible to know if the requirement is met. In this study, we report all $g_{c,ET}$ values, regardless of assumably high daytime evaporation.

COS-based transpiration (T_{COS}) was calculated from the canopy conductance (Eq. (4)) as in Berkelhammer et al. (2020)

$$T_{COS} = g_{c,COS} VPD \quad (5)$$

and COS-based evaporation (E_{COS}) by subtracting T_{COS} (Eq. (5)) from the total evapotranspiration (ET)

$$E_{COS} = ET - T_{COS}. \quad (6)$$

Another ET partitioning method, the conditional eddy covariance (CEC) method proposed by Zahn et al. (2022), was also tested to validate the COS-based transpiration estimate. In the CEC method, raw EC data are divided into quadrants based on the turbulent fluctuations of vertical wind (w'), CO_2 (c') and H_2O (q') such that concurrent $w' > 0$, $c' > 0$ and $q' > 0$ indicate soil respiration and evaporation (E_{CEC}), while simultaneous $w' > 0$, $c' < 0$ and $q' > 0$ indicate CO_2 uptake (GPU) and transpiration (T_{CEC}). In an earlier study, the CEC method performed best out of three different ET partitioning methods tested against independent estimates in a grassland in Kenya (Zahn et al., 2022) and was thus chosen for this study.

A third canopy conductance estimate, based on the CEC method ($g_{c,CEC}$), was then calculated by inverting Eq. (5) and using T_{CEC} as the transpiration estimate.

3. Results

3.1. Environmental conditions

The measurement campaign from 23 Nov to 21 Dec 2019 took place during the short wet season (Fig. 1). The mean air temperature was 26.4 °C during daytime and 21.2 °C during nighttime (Fig. 2) The maximum T_{air} of 31.8 °C was reached on 4 Dec in the afternoon, while the minimum T_{air} of 17.9 °C was measured in the same morning before sunrise. Soil temperature measured in a sun-exposed location ($T_{soil,exposed}$) was always higher (median of 25.5 °C) than the soil temperature at a shaded location ($T_{soil,shaded}$; median 22.4 °C). The maximum soil temperatures were 43.3 °C on 19 Dec noon and 38.1 °C on 25 Nov afternoon for the exposed and shaded locations, respectively. Minimum soil temperatures were 21.7 °C on 23 Nov evening and 16.8 °C on 25 Nov morning before sunrise for the exposed and shaded locations, respectively. Daytime maximum PAR varied from 1546 to 2374 μmol m^{-2} s^{-1}. Total precipitation from 30 Nov (when precipitation measurements on site started) to 21 Dec was 59 mm, while maximum daily precipitation was 15 mm on 1 Dec. Total precipitation during the whole measurement period, when including precipitation measurements from the nearby weather stations for the first 7 days was 123 mm (23 Nov to 21 Dec). SWC had its maximum value of 0.24 m^3 m^{-3} in the beginning of the measurements and slowly decreased during the campaign to its minimum of 0.09 m^3 m^{-3} on the

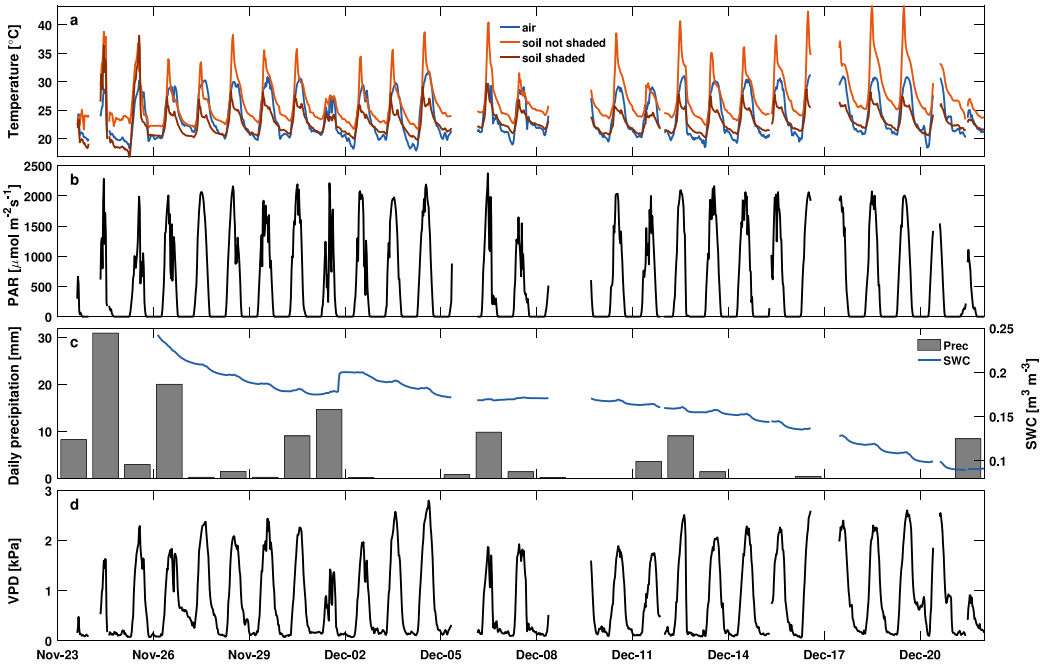

Fig. 1. Meteorological conditions during the measurement campaign 23 Nov–21 Dec 2019: air (blue) and soil temperatures (sun exposed soil in orange, shaded soil in red) (a), photosynthetically active radiation (*PAR*; b), daily rainfall (black bars) and soil water content (*SWC*, blue line; c), and vapor pressure deficit (*VPD*; d).

last campaign day. A maximum *VPD* of 2.8 kPa was observed together with maximum air temperature on 4 Dec during the day, while the minimum of 0.06 kPa was observed on 16 Dec during the night. Median *VPD* during the campaign was 0.4 kPa. Local wind conditions closely followed the permanent regional east-to-west prevailing trade winds, typically coming from 60–90° directions. Maximum wind speed was 4.8 m s^{-1}, with the median of 1.6 m s^{-1}.

3.2. COS fluxes and their drivers

The ecosystem showed net COS as well as CO_2 uptake during the measurement period 23 Nov–21 Dec (Fig. S3), with median (and 25th and 75th percentiles) nighttime EC fluxes of $-11.5^{+3.6}_{-3.4}$ pmol m^{-2} s^{-1} and $-2.70^{+2.11}_{-1.94}$ μmol m^{-2} s^{-1} for COS and CO_2, respectively, and daytime fluxes of $-5.6^{+13.2}_{-14.6}$ pmol m^{-2} s^{-1} and $0.46^{+1.47}_{-0.82}$ μmol m^{-2} s^{-1} for COS and CO_2, respectively (Fig. 2c). The COS fluxes were statistically different from zero ($p < 0.05$, tested with t-test) both during daytime and nighttime. The measurements thus showed the typical CAM gas exchange patterns with higher uptake at night than during the day for both COS and CO_2. Moreover, the four CAM gas exchange phases (Osmond, 1978) were visible for both COS and CO_2 fluxes, with high COS (−11.0 ± 10.0 pmol m^{-2} s^{-1}) and CO_2 (−1.59 ± 2.90 μmol m^{-2} s^{-1}) uptake at night (phase I, determined from sunset at 18:00 until sunrise at 6:00), increased COS (−17.0 ± 14.8 pmol m^{-2} s^{-1}) and CO_2 (−1.26 ± 3.34 μmol m^{-2} s^{-1}) uptake right after sunrise (phase II, at 6:00–9:00, determined from sunrise until *PAR* > 1000 μmol m^{-2} s^{-1}), very low or close to zero exchange rates of COS (−7.1 ± 18.0 pmol m^{-2} s^{-1}) and CO_2 (0.41 ± 2.90 μ mol m^{-2} s^{-1}) in the mid-photoperiod (phase III, from approx. 9:00 to 15:00, determined from end of phase II until *PAR* < 1000 μmol m^{-2} s^{-1}), followed by low but steadily increasing uptake rates of COS (−11.1 ± 12.3 pmol m^{-2} s^{-1}) and CO_2 (−3.22 ± 3.35 μmol m^{-2} s^{-1}) observed in the late afternoon (phase IV, 15:00 to 18:00, determined from end of phase III until sunset). The highest net uptake at hourly time resolution was observed at 6:00 ($-16.2^{-11.3}_{-18.2}$ pmol m^{-2} s^{-1}) for COS and at 20:00 ($-5.06^{-1.16}_{-6.12}$ μmol m^{-2} s^{-1}) for CO_2, while the lowest COS uptake was observed at 10:00 ($-1.4^{2.7}_{-10.3}$ pmol m^{-2} s^{-1}) and highest net emission of CO_2 at 13:00 ($1.56^{2.53}_{0.30}$ μmol m^{-2} s^{-1}). Gross CO_2 uptake *GPU*, modeled with RF, was also higher during nighttime than daytime, but did not go to zero during the wet season, even during daytime (Fig. S4). Moreover, the nighttime *GPU* was of similar magnitude both during the dry and wet seasons. The mean fluxes over the whole measurement period were −8.9 ± 13.9 pmol m^{-2} s^{-1} for COS and −1.16 ± 3.19 μmol m^{-2} s^{-1} for CO_2. The ratio of COS to CO_2 deposition velocities, i.e., the median ecosystem relative uptake (*ERU*), was 1.7 in the night and 0.88 during daytime under high radiation (*PAR* > 700 μmol m^{-2} s^{-1}).

Opaque soil chamber measurements showed a small soil COS sink (−0.1 ± 0.5 pmol m^{-2} s^{-1} on average), while transparent chambers always resulted in COS emissions (0.6 ± 0.7 pmol m^{-2} s^{-1} on average). Overall, the soil was a small source of COS to the atmosphere (0.3 ± 0.8 pmol m^{-2} s^{-1}; Fig. S5). Assuming homogeneous soil fluxes in the EC footprint area, the soil contributed 2.6% to nighttime and 5.4% to daytime ecosystem fluxes. Moreover, the vegetated surface emitted more COS under radiation (1.1 ± 0.9 pmol m^{-2} s^{-1}) than the bare soil (0.4 ± 0.5 pmol m^{-2} s^{-1}). Soil COS emissions increased with radiation (from 0.1 pmol m^{-2} s^{-1} at *PAR* = 0 μmol m^{-2} s^{-1} to approx. 1 pmol m^{-2} s^{-1} at *PAR* > 1500 μmol m^{-2} s^{-1}), and also with temperature (from 0.2 pmol m^{-2} s^{-1} at T_{air} < 30 °C to 1.4 pmol m^{-2} s^{-1} at T_{air} > 40 °C in the transparent chamber, and from −0.04 pmol m^{-2} s^{-1} at T_{air} < 30 °C to 0.3 pmol m^{-2} s^{-1} at T_{air} > 40 °C in the dark chamber; Fig. 3f,h).

Increasing T_{air}, *VPD* and *PAR* decreased the COS uptake also at ecosystem scale (from −17 pmol m^{-2} s^{-1} at *VPD* < 0.2 kPa, T_{air} < 22 °C and *PAR* < 100 μmol m^{-2} s^{-1} to nearly zero flux at *VPD* > 2 kPa, T_{air} > 29 °C and *PAR* > 1300 μmol m^{-2} s^{-1}) but increased soil COS emissions (Fig. 3). Occasional ecosystem scale emissions were observed at high T_{air} and *VPD* during daytime (in total 36% of daytime data), while during nighttime, only few data points of COS emission were observed (8% of nighttime data). However, increasing T_{air} during rain events increased COS uptake (Fig. S6).

The most important drivers of COS fluxes at the ecosystem scale were $T_{soil,exposed}$, *PAR*, T_{air}, *SWC* and *VPD* according to the RF model (with variable importance of 0.23, 0.18, 0.16, 0.15, 0.15, respectively; Table S1). When the model was trained on nighttime data only, the most important variables were *VPD*, T_{air}, *SWC* and $T_{soil,exposed}$ (variable importance of 0.25, 0.23, 0.20, 0.19, respectively), while for

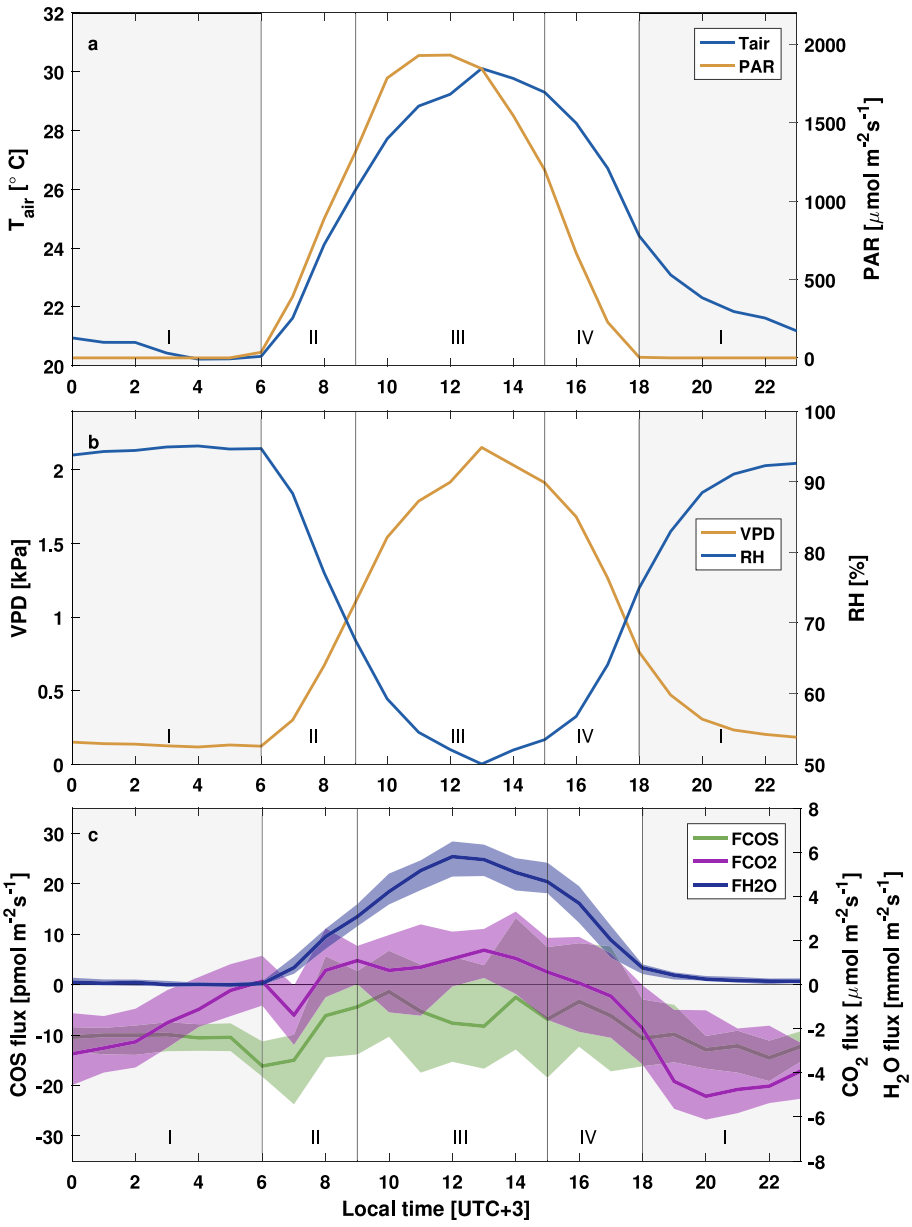

Fig. 2. Median diel variations of (a) air temperature (T_{air}, blue, left axis) and photosynthetically active radiation (*PAR*, orange, right axis), (b) vapor pressure deficit (*VPD*; orange, left axis) and relative humidity (*RH*, blue, right axis), and (c) COS (green), CO_2 (purple) and H_2O (dark blue) fluxes and their 25th and 75th percentiles (shaded areas). The gray area represents nighttime and vertical black lines indicate the four CAM gas exchange phases (roman numerals; see text for details).

the daytime-trained model, most relevant variables were T_{air}, *SWC*, *PAR* and $T_{soil,shaded}$ (variable importance of 0.19, 0.16, 0.18, 0.18, respectively).

SHAP analysis revealed that low T_{air} (< 21 °C) decreased nighttime COS uptake (positive SHAP value), while high T_{air} (> 24 °C) decreased both daytime and nighttime COS uptake (Fig. 4). Higher soil moisture (*SWC* > 0.15 m^3 m^{-3}) increased both nighttime and daytime COS uptake (negative SHAP values), while very high *SWC* values (*SWC* > 0.20 m^3 m^{-3} during day and *SWC* > 0.23 m^3 m^{-3} during night) decreased COS uptake. *VPD* was mostly limiting COS uptake during nighttime and had a stronger net effect on the COS flux than during daytime (Fig. S7). A clear threshold value for *VPD* limitation was found at *VPD* > 0.6 kPa at nighttime (SHAP value turned positive, i.e., indicating limited COS uptake), while during the day, the limit was higher at *VPD* > 2.2 kPa. *SWC* increased COS uptake in the beginning of the campaign, but as *SWC* decreased, it started to limit COS uptake. Towards the end of the measurement period, after a rain event on 20 Dec, the SHAP value of *SWC* started to have negative values again, indicating increased COS uptake.

3.3. Canopy stomatal conductance and water fluxes

Canopy stomatal conductance $g_{c,COS}$ was lower than $g_{c,ET}$ during daytime (on average 0.03 ± 0.1 and 0.24 ± 0.16 mol m^{-2} s^{-1} for $g_{c,COS}$ and $g_{c,ET}$, respectively), but both conductances agreed well during nighttime (on average 0.06 ± 0.05 and 0.08 ± 0.13 mol m^{-2} s^{-1} for $g_{c,COS}$ and $g_{c,ET}$, respectively; Fig. 5). Canopy stomatal conductance inferred from the CEC method $g_{c,CEC}$ showed higher conductance values in the CAM phases II and IV, like $g_{c,COS}$ and $g_{c,ET}$. However, there were no statistical differences in the midday $g_{c,CEC}$ (0.06 ± 0.25) to nighttime $g_{c,CEC}$ (0.09 ± 0.44; $p = 0.04$). Nighttime $g_{c,CEC}$ showed similar, although slightly lower values than both $g_{c,COS}$ and $g_{c,ET}$

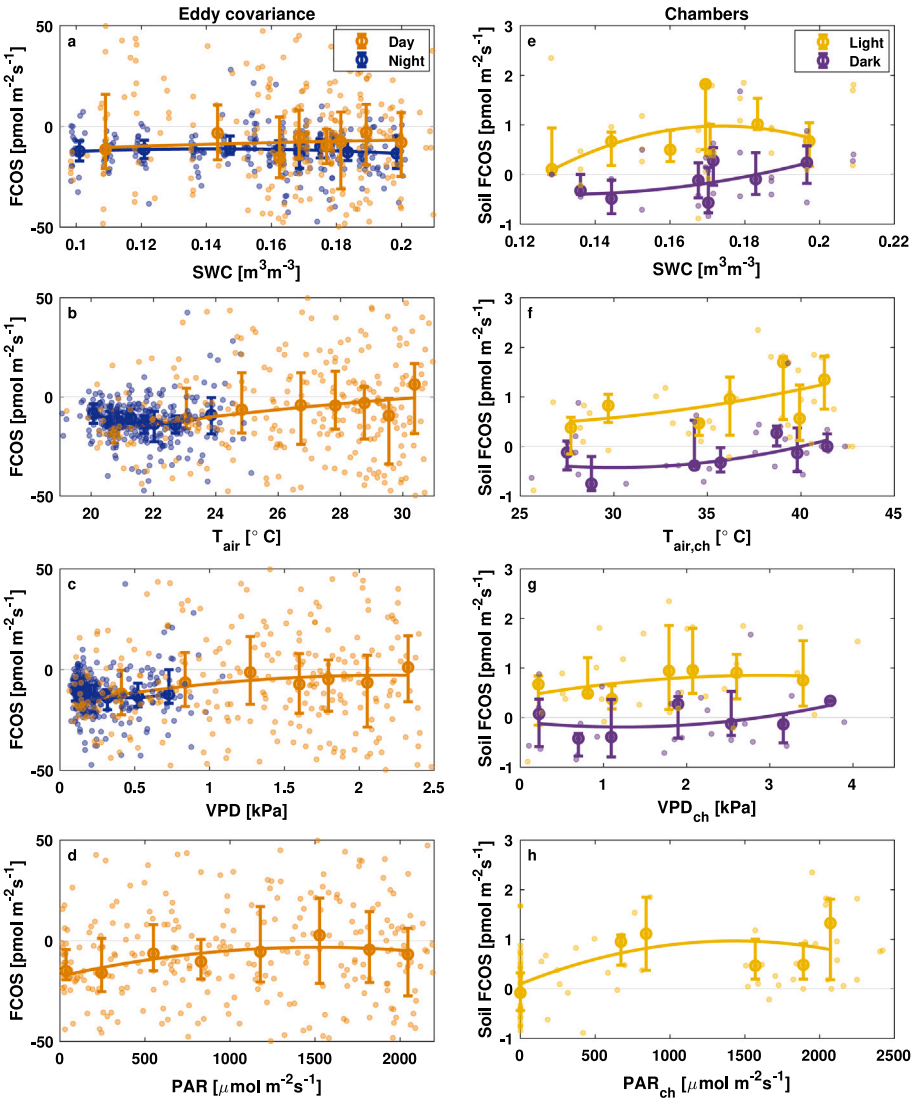

Fig. 3. COS fluxes (*FCOS*) measured with eddy covariance (EC; a–d) and soil chambers (ch; e–h) against environmental drivers: soil water content (*SWC*; a, e), air temperature (T_{air}; b, f), vapor pressure deficit (*VPD*; c, g) and photosynthetically active radiation (*PAR*; d, h). Data are separated into daytime (orange) and nighttime (blue) EC measurements, as well as between transparent daytime chamber (yellow) and daytime opaque chamber (purple) measurements. Data are binned to 7 or 8 equally sized bins, with each bin containing 35 datapoints for EC or 5 for chambers fluxes. Error bars represent the 25th and 75th percentiles, fit lines are based on second order polynomial functions.

while daytime $g_{c,CEC}$ was similar to $g_{c,COS}$. Daytime and nighttime $g_{c,COS}$ differed statistically ($p < 0.001$, tested with t-test). Transpiration inferred from FCOS measurements and from the CEC method agreed well on a diel scale, although the CEC method showed always higher transpiration and lower evaporation than the COS method (Fig. 6). Nighttime *T/ET* was higher (0.66 ± 0.46) than *E/ET* (0.34 ± 0.46) for the CEC method, while the COS-based method showed higher nighttime *E/ET* (0.59 ± 0.42) than *T/ET* (0.41 ± 0.53). When *VPD* > 0.5 kPa, the nighttime *T/ET* fractions were highest at 0.45 ± 0.29 and 0.81 ± 0.30 for CEC and COS methods, respectively. During daytime, both methods showed that evaporation dominated over transpiration, with *E/ET* being 0.79 ± 0.09 and 0.88 ± 0.20 with CEC and COS-based methods, respectively, while *T/ET* was 0.21 ± 0.17 and 0.12 ± 0.23 with the CEC and COS-based methods, respectively. Evaporation calculated from soil chamber water fluxes was close to both ecosystem scale estimates, giving further proof for both *ET* partitioning methods (Fig. S8). Transpiration fraction *T/ET* increased with decreasing *VPD* during the day, while low *VPD* reduced transpiration in the night (Fig. 6c). On the other hand, evaporation fraction *E/ET* decreased with decreasing *VPD* during the day and increased during the night. *WUE*, calculated as $WUE = GPU/T$, was 69 ± 34 μmol CO_2 (mmol H_2O)$^{-1}$ during nighttime and 3.9 ± 9.8 μmol CO_2 (mmol H_2O)$^{-1}$ during daytime (Fig. S9), while the median over the whole measurement period was 23 ± 46 μmol CO_2 (mmol H_2O)$^{-1}$. To better compare with previous ecosystem scale studies, we also calculated *WUE* as $WUE_{NET} = NEE/ET$. WUE_{NET} had a median nighttime value of 7.3 ± 8.1 μmol CO_2 (mmol H_2O)$^{-1}$ and daytime value of 0.1 ± 0.29 μmol CO_2 (mmol H_2O)$^{-1}$.

4. Discussion

4.1. Temporal patterns of COS fluxes and their drivers

The observed COS fluxes of the sisal plantation in Kenya during the short wet season were of the same magnitude as non-growing-season fluxes observed at a boreal forest (Vesala et al., 2022), a wheat field (Maseyk et al., 2014), and of a prairie and a maize field (Berkelhammer et al., 2020). However, the fluxes from the sisal plantation in this study were less than half of the magnitude of fluxes observed during the peak growing seasons in Vesala et al. (2022), Berkelhammer et al. (2020) and Maseyk et al. (2014), as well as those reported in a

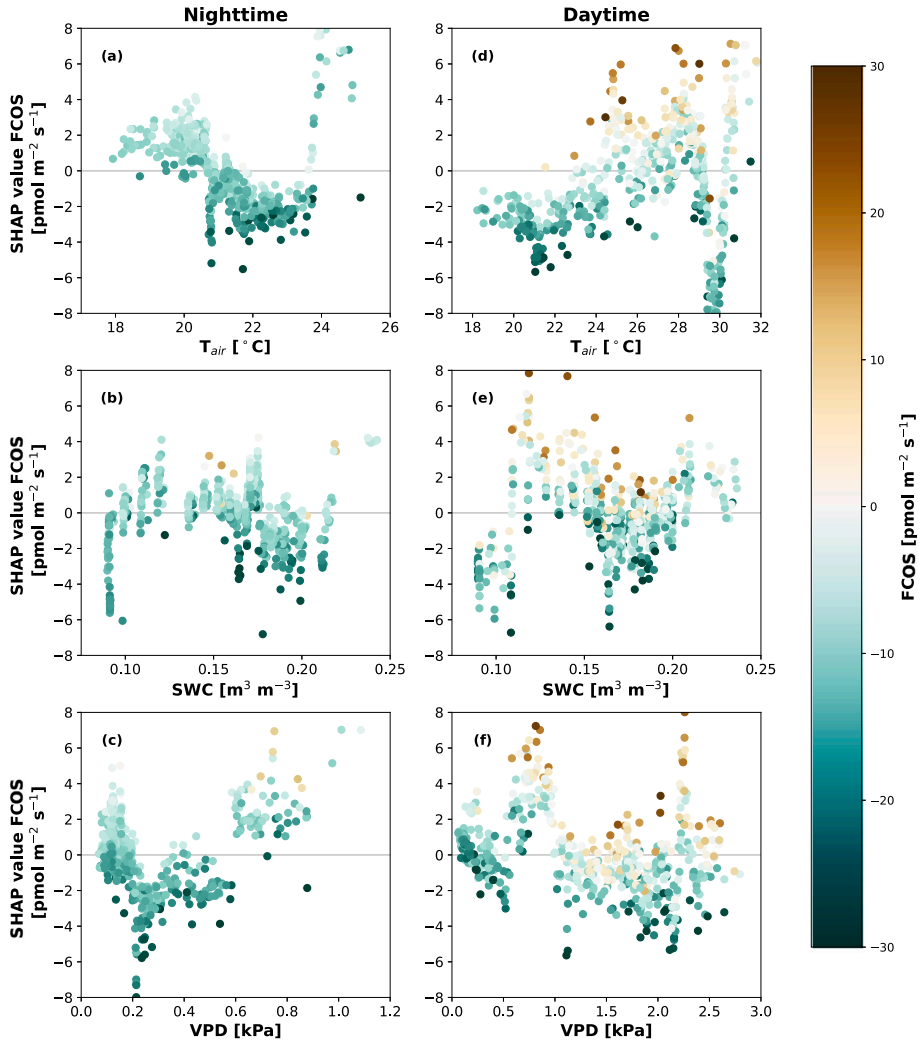

Fig. 4. Shapley additive explanation (SHAP) values of T_{air}, *SWC* and *VPD* based on random forest (RF) model for COS flux (*FCOS*) during nighttime (a–c) and daytime (d–f). Colors represent the modeled *FCOS*. Negative SHAP values indicate increased COS uptake or decreased COS emissions, while positive SHAP values indicate decreased net COS uptake or increased COS emissions. Note the different scaling of the x-axes for T_{air} and *VPD*.

temperate mountain grassland, a Mediterranean savanna, a temperate beech forest and a soybean field (Spielmann et al., 2019). The low uptake of sisal compared to C_4 and C_3 plants measured in other studies could be explained by the prevailing semi-arid and low soil moisture conditions, despite the wet season (Oct to Dec) when most growth is to be expected, since the wet season was transitioning into dry season (Skogberg et al., 2025). Moreover, the *ERU* value found in this study (1.7 in the night, 0.88 in the day) was lower than that reported in previous studies (2.9 ± 1.7 in Asaf et al. (2013) and 3.3 ± 1.1 in Maseyk et al. (2014)), indicating lower relative COS uptake compared to CO_2 uptake. This may indicate differences in the biochemical COS uptake in CAM plants compared to C_4 and C_3 plants. *ERU* is a useful metric to obtain *GPP* estimates at regional to continental scales using atmospheric COS and CO_2 concentration measurements (Campbell et al., 2008).

The soil COS fluxes were of similar magnitude as those observed in an agricultural field (Maseyk et al., 2014) and in a grassland Berkelhammer et al. (2014). Increasing soil COS emissions under high temperatures and radiation in agricultural land have also previously been observed by Maseyk et al. (2014) and Kitz et al. (2020). Since the soil contribution to the ecosystem scale COS fluxes was negligible, this highlights the potential of using ecosystem scale COS fluxes as a tracer for canopy stomatal conductance and thus also carbon uptake in the arid region.

In this study, the diel cycle of the COS flux closely followed that of the CO_2 flux. Both revealed the typical CAM gas exchange pattern (Osmond, 1978), with highest uptake observed in the night during phase I, a strong uptake right after sunrise in the beginning of phase II, reduced uptake (or net emission in the case of CO_2 flux) in phase III during midday, and a transitioning phase in the late afternoon in phase IV before sunset. In many species, CAM photosynthesis occurs together with C_3 photosynthesis, which only occurs during daytime, demonstrating a large degree of functional plasticity in response to water stress (Cushman, 2001; Winter, 2019). However, *Agave* species have generally been found to be constitutive CAM, i.e., almost completely CAM plants (Winter, 2019), although they can also respond to high water availability in the wet season with added daytime C_3 photosynthesis (Skogberg et al., 2025). Since the ecosystem scale COS fluxes were more negative than the simultaneous daytime soil COS fluxes, our data indicated also daytime stomatal COS uptake during the wet season. This was further supported by the *GPU* estimate that remained at the same level during wet and dry seasons during nighttime (Skogberg et al., 2025), while the wet season daytime *GPU* was higher than dry season daytime *GPU*, which was very small. This clearly showed that the sisal stomata remained open during daytime in the wet season, maintaining both C_3 and CAM photosynthesis.

Air temperature was a more important driver than the soil temperature, which suggested a stomatal limitation on COS fluxes because

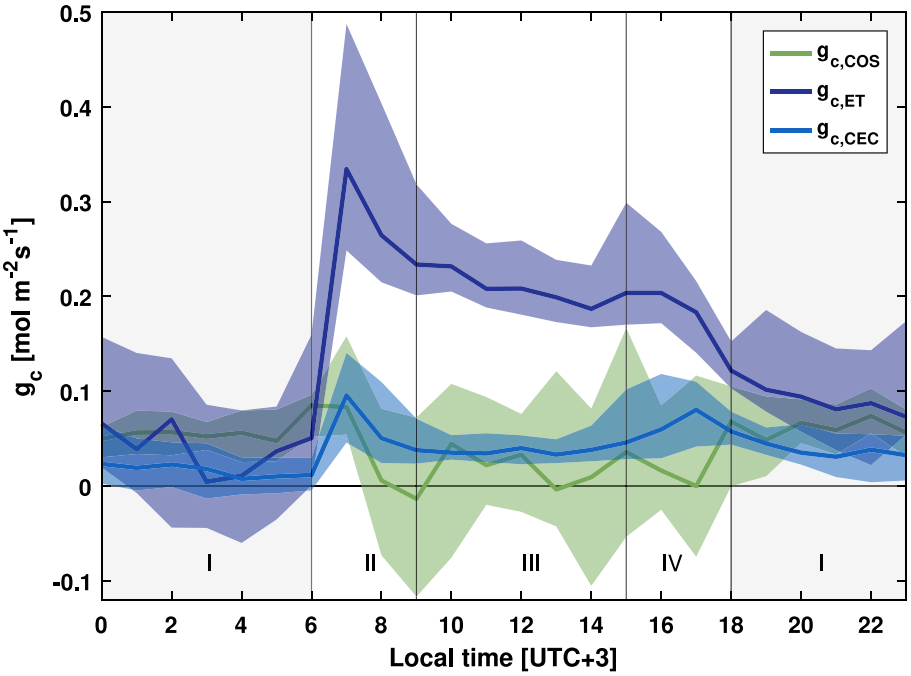

Fig. 5. Diel variation of canopy stomatal conductance calculated from COS ($g_{c,COS}$, green; Eq. (4)) and H_2O ($g_{c,ET}$, dark blue; see Section 2.6 for details) flux measurements as well as from the conditional eddy covariance (CEC) method ($g_{c,CEC}$; blue). The gray area represents nighttime and vertical black lines indicate the four CAM gas exchange phases (roman numerals; see text for details).

stomata are more influenced by changes in atmospheric conditions than in the soil (Göbel et al., 2019). *VPD* was an important driver both during daytime and nighttime, again indicating stomatal limitation (Kooijmans et al., 2019). The SHAP analysis implied that stomata were closed during the day when T_{air} was high, and that stomata were closed during night with low T_{air} and limited COS uptake. In contrast, Owen et al. (2016) found increased CO_2 uptake during cold nights for a different *Agave* species, *Agave tequilana*, pointing towards higher stomatal activity. Low soil moisture was limiting both daytime and nighttime COS uptake. This limitation is due to low CA activity under dry soil conditions (Kevrešan et al., 1997), restraining the hydrolysis reaction and thus COS uptake. High soil moisture in our study, on the other hand, limited daytime COS uptake, likely due to heavy rain events temporarily reducing COS uptake through reduced stomatal conductance.

4.2. COS as proxy for canopy conductance and transpiration

Canopy conductances inferred from COS and H_2O fluxes followed opposite diel cycles, with $g_{c,COS}$ having its maximum values at night but $g_{c,ET}$ having its maximum during the day, while $g_{c,CEC}$ followed the diurnal cycle of $g_{c,COS}$. Transpiration fraction was higher during night than during day, as expected for a CAM ecosystem. The daytime difference in $g_{c,COS}$ and $g_{c,ET}$ was likely due to high *E/ET* fractions, since assumptions underlying $g_{c,ET}$ rely on negligible *E* (Wehr and Saleska, 2021). Moreover, $g_{c,CEC}$, that was based on transpiration estimate, did not show high daytime values. However, since both $g_{c,ET}$ and $g_{c,CEC}$ agreed well with $g_{c,COS}$ during the night when *T/ET* fraction was at its highest, the COS-based conductance estimate seems reasonable. The magnitude of the nighttime g_c was similar, although slightly lower than observed in Wehr et al. (2017) for a temperate deciduous forest during daytime (0.1 mol m^{-2} s^{-1}) and slightly higher than (modeled) canopy conductance values for a pineapple field in the wet season (San-José et al., 2007). The COS-based transpiration estimate followed a similar diel cycle as the CEC-based estimate but was consistently lower than the CEC-based transpiration. Daytime transpiration was low with both methods. However, as our *GPU* estimate showed gross CO_2 uptake also during the day (Fig. S4), it is likely that the very low COS-based transpiration estimate was underestimated, especially during the day. Moreover, atmospheric T_{air} and *VPD*, used in the COS-based calculation of $g_{c,COS}$ and T_{COS}, were probably different from leaf temperature and *VPD* experienced by the sisal leaves. Leaf temperatures are typically higher than T_{air} (Schulze et al., 2019), and thus COS-based $g_{c,COS}$ and T_{COS} likely underestimated (Vesala et al., 2005). Moreover, since there are no studies on mesophyll COS conductance in CAM plants, we assumed it to be similar as for C_3 plants, i.e., higher than stomatal conductance (Kooijmans et al., 2019; Sun et al., 2024) and was thus ignored in the total conductance calculation. Using a constant atmospheric mixing ratio of COS in estimating $g_{c,COS}$ adds to the uncertainty of the method. However, we tested using both higher (500 ppt) and lower (300 ppt) mixing ratios in the $g_{c,COS}$ calculation, but the results were within the uncertainty of the original $g_{c,COS}$, with constant COS mixing ratio of 394 ppt (Fig. S10). Both *ET* partitioning methods showed very low transpiration during nighttime at high humidity, as expected. If mesophyll conductance would limit COS exchange, the T_{COS} estimate would also decrease, while the COS-independent T_{CEC} estimate would not. However, we did not observe higher limitations in the COS-based T_{COS} estimate compared to the CEC-based T_{CEC} even in dry conditions. This indicated that the mesophyll conductance did not start to limit COS uptake even in dry conditions, unlike observed in Wohlfahrt et al. (2018) and Sun et al. (2024). This further highlighted the higher drought resilience of sisal compared to the Mediterranean pine forest and coast live oak studied by Wohlfahrt et al. (2018) and Sun et al. (2024), respectively.

4.3. Water use of sisal

Nighttime *WUE* (defined as $WUE = GPU/T$) of 68 μmol CO_2 (mmol $H_2O)^{-1}$ was higher than *WUE* values reported for CAM plants in earlier (laboratory) studies (4–10 μmol CO_2 (mmol $H_2O)^{-1}$ in Borland et al. (2009)) and 6–30 μmol CO_2 (mmol $H_2O)^{-1}$ in Lüttge (2004)). However, average *WUE* calculated over 24 h (35 μmol CO_2 (mmol $H_2O)^{-1}$) was

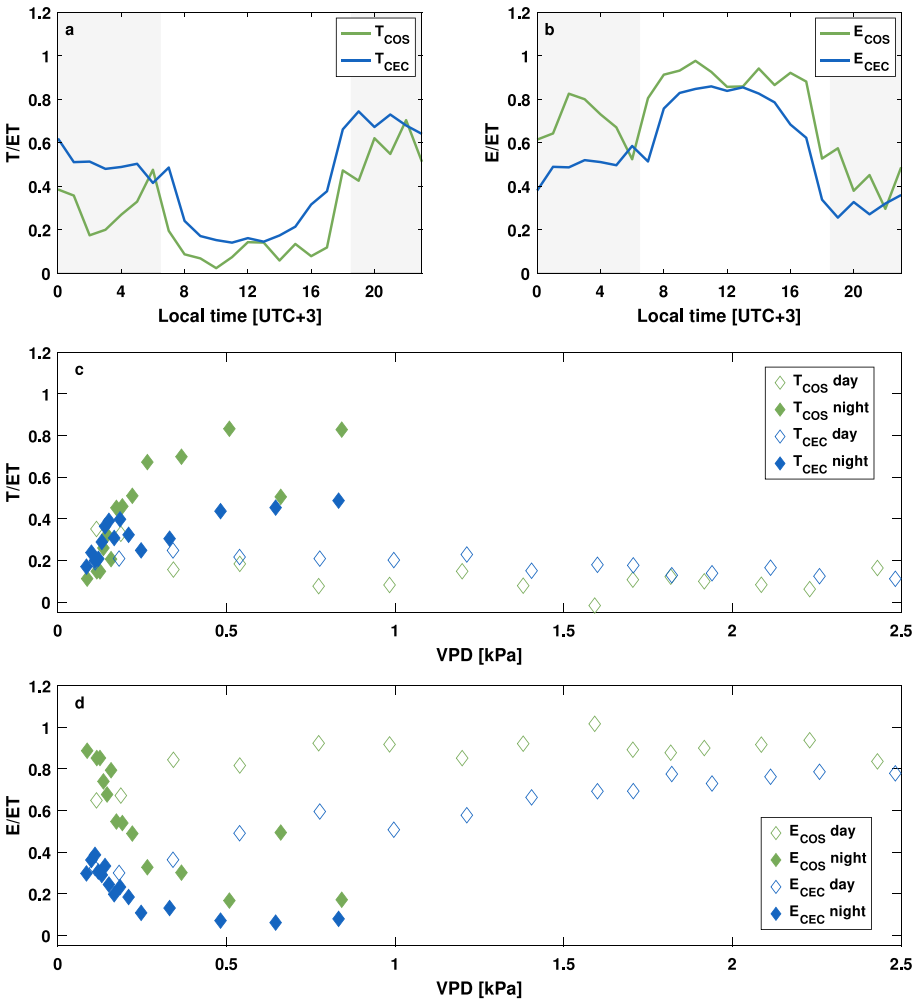

Fig. 6. Diel variation of (a) transpiration (*T/ET*) and (b) evaporation (*E/ET*) fractions, inferred from *FCOS* measurements (green) and from the conditional eddy covariance (CEC) method (blue; see Section 2.7 for details). The gray shaded area represents nighttime. Dependence of *T/ET* and *E/ET* fractions on vapor pressure deficit (*VPD*; c, d). Data in subplots c and d are binned to 15 equally sized bins.

very similar to what was reported in a laboratory study in Eller and Ferrari (1997) (up to 42 μmol CO_2 (mmol H_2O)$^{-1}$). *WUE* changes with the CAM phase, with lowest *WUE* observed in phase IV (Lüttge, 2004), as also observed in our study. Daytime *WUE* of 3.9 μmol CO_2 (mmol H_2O)$^{-1}$, on the other hand, was comparable to *WUE* of C_3 plants (Borland et al., 2009), again highlighting the photosynthetic plasticity of sisal during the wet season and good water availability. The ecosystem WUE_{NET} (7.3 μmol CO_2 (mmol H_2O)$^{-1}$), on the other hand, was very similar to the 6.9 μmol CO_2 (mmol H_2O)$^{-1}$ reported by Owen et al. (2016) for *Agave tequilana* during nighttime in the wet season. Due to the high *WUE* observed in CAM plants, they are essential in mitigating climate change in arid regions (Yang et al., 2015; Borland et al., 2015). Moreover, it has been suggested that the CAM traits could be added to C_3 crops through bioengineering to increase *WUE*, drought resilience and crop yields (Yang et al., 2024; Winter and Smith, 2022). Since sisal as a future fiber plant is expected to increase in relevance to a more sustainable, green economy (Islam et al., 2025; Kozłowski et al., 2020), studies about CAM plants and ecosystems are critical also for their representation in regional and global carbon models. *WUE* serves as a bridge between water and carbon cycles and solving *WUE* for CAM plants helps in modeling the water–carbon relations in arid regions (Stoy et al., 2019). It further helps with scaling between remote sensing and *in-situ* data in bottom-up estimates and, e.g., evaluating model performance. Field studies reporting *WUE* for arid ecosystems are thus crucial for further development of land surface models.

5. Conclusions

COS fluxes measured over *A. sisalana* showed the CAM-typical diel gas exchange pattern with higher uptake observed at night than during the day. However, the uptake continued also under radiation, indicating the combination of CAM and C_3 photosynthesis of the sisal plantation during the wet season. Ecosystem COS fluxes were mostly controlled by stomatal closure. Soil COS fluxes were negligible compared to ecosystem scale fluxes but increased under high radiation and temperature. Our results show that COS fluxes provide reliable estimates for canopy stomatal conductance as well as for *ET* partitioning, also for CAM plant-dominated ecosystems. The negligible soil COS fluxes further encourage the use of COS fluxes as a tracer for ecosystem and regional scale CO_2 uptake in arid regions. For future studies, the dataset presented in this study allows better parameterization of CAM gas exchange and productivity in models. As sisal cultivation is expected to increase, representation of CAM plants becomes more important in regional and global models. In order to include CAM plant COS, CO_2 and water exchange in land surface models, further studies on CAM using COS as a tracer for conductance are needed to properly parameterize CAM plant environmental responses. Chamber enclosures or laboratory measurements would further provide valuable insights into the mesophyll conductance of CAM. Such efforts would greatly advance the understanding of arid region water and carbon cycle responses to climate variability.

CRediT authorship contribution statement

Kukka-Maaria Kohonen: Writing – original draft, Visualization, Validation, Methodology, Investigation, Formal analysis, Data curation, Conceptualization. **Angelika Kübert:** Writing – review & editing, Formal analysis, Conceptualization. **Lutz Merbold:** Writing – review & editing, Resources, Funding acquisition. **Matti Räsänen:** Writing – review & editing, Resources, Data curation. **Nina Buchmann:** Writing – review & editing, Funding acquisition. **Ivan Mammarella:** Writing – review & editing, Supervision, Methodology, Conceptualization. **Petri Pellikka:** Writing – review & editing, Resources, Project administration, Funding acquisition. **Timo Vesala:** Writing – review & editing, Supervision, Resources, Project administration, Funding acquisition, Conceptualization.

Declaration of competing interest

The authors declare the following financial interests/personal relationships which may be considered as potential competing interests: Given their role as editorial board members, Prof. Timo Vesala and Dr. Lutz Merbold had no involvement in the peer review of this article and had no access to information regarding its peer review. Full responsibility for the editorial process for this article was delegated to another journal editor. If there are other authors, they declare that they have no known competing financial interests or personal relationships that could have appeared to influence the work reported in this paper.

Acknowledgments

We want to thank Sami Haapanala and the staff at the Taita Research Station of the University of Helsinki, especially Mwadime Mjomba for constructing the base for the measurement station as well as for helping with station maintenance and set up, and Muhia Gicheru and Ambrose Nyga for setting up the measurement station. We also want to thank the very helpful staff at the International Livestock Research Institute (ILRI), especially George Wanyama, for assisting with shipping of instruments and ordering gas bottles. We would like to thank the Teita sisal estate for making it possible for us to conduct the study and for supporting us with logistics and electricity. Without their interest and cooperation, our study would not have been possible. We thank Mikko Skogberg for chamber flux calculations. Research permission from NACOSTI (no. P/18/97336/26355) is acknowledged.

The setup of the measurement campaign was funded by the Research Council of Finland for SMARTLAND (Environmental sensing of ecosystem services for developing a climate-smart landscape framework to improve food security in East Africa, decision no. 318645) for TV and PP. The research was funded by University of Helsinki (ICOS-Finland). LM acknowledges funding received from the European Union's Horizon Europe Programme (grant agreement number 101058525) for the project "Knowledge and climate services from an African observation and Data research Infrastructure (KADI)".

Appendix A. Supplementary data

Supplementary material related to this article can be found online at https://doi.org/10.1016/j.agrformet.2025.110966.

Data availability

Data used in this manuscript are publicly available at https://doi.org/10.5281/zenodo.17855873 and https://doi.org/10.5281/zenodo.14445518.

References

Asaf, D., Rotenberg, E., Tatarinov, F., Dicken, U., Montzka, S.A., Yakir, D., 2013. Ecosystem photosynthesis inferred from measurements of carbonyl sulphide flux. Nat. Geosci. 6, 186–190. http://dx.doi.org/10.1038/NGEO1730.

Millennium ecosystem assessment, M., 2005. Ecosystems and human well-being, vol. 5, Island press Washington, DC.

Aubinet, M., Grelle, A., Ibrom, A., Rannik, Ü., Moncrieff, J., Foken, T., Kowalski, A.S., Martin, P.H., Berbigier, P., Bernhofer, C., Clement, R., Elbers, J., Granier, A., Grünwald, T., Morgenstern, K., Pilegaard, K., Rebmann, C., Snijders, W., Valentini, R., Vesala, T., 2000. Estimates of the annual net carbon and water exchange of forests: the EUROFLUX methodology. Adv. Ecol. Res. 30, 113–175.

Aubinet, M., Vesala, T., Papale (eds.), D., 2012. Eddy Covariance: a Practical Guide to Measurement and Data Analysis. Springer Science & Business Media.

Berkelhammer, M., Alsip, B., Matamala, R., Cook, D., Whelan, M., Joo, E., Bernacchi, C., Miller, J., Meyers, T., 2020. Seasonal evolution of canopy stomatal conductance for a prairie and maize field in the midwestern United States from continuous carbonyl sulfide fluxes. Geophys. Res. Lett. 47 (6), http://dx.doi.org/10.1029/2019GL085652, e2019GL085652.

Berkelhammer, M., Asaf, D., Still, C., Montzka, S., Noone, D., Gupta, M., Provencal, R., Chen, H., Yakir, D., 2014. Constraining surface carbon fluxes using in situ measurements of carbonyl sulfide and carbon dioxide. Glob. Biogeochem. Cycles 28 (2), 161–179.

Borland, A.M., Griffiths, H., Hartwell, J., Smith, J.A.C., 2009. Exploiting the potential of plants with crassulacean acid metabolism for bioenergy production on marginal lands. J. Exp. Bot. 60 (10), 2879–2896. http://dx.doi.org/10.1093/jxb/erp118.

Borland, A.M., Wullschleger, S.D., Weston, D.J., Hartwell, J., Tuskan, G.A., Yang, X., Cushman, J.C., 2015. Climate-resilient agroforestry: physiological responses to climate change and engineering of crassulacean acid metabolism (CAM) as a mitigation strategy. Plant Cell Environ. 38 (9), 1833–1849. http://dx.doi.org/10.1111/pce.12479.

Campbell, J.E., Carmichael, G.R., Chai, T., Mena-Carrasco, M., Tang, Y., Blake, D.R., Blake, N.J., Vay, S.A., Collatz, G.J., Baker, I., Berry, J.A., Montzka, S.A., Sweeney, C., Schnoor, J.L., Stanier, C.O., 2008. Photosynthetic control of atmospheric carbonyl sulfide during the growing season. Science 322 (5904), 1085–1088. http://dx.doi.org/10.1126/science.1164015.

Cushman, J.C., 2001. Crassulacean acid metabolism. a plastic photosynthetic adaptation to arid environments. Plant Physiol. 127 (4), 1439–1448. http://dx.doi.org/10.1104/pp.010818.

Eller, B., Ferrari, S., 1997. Water use efficiency of two succulents with contrasting CO_2 fixation pathways. Plant Cell Environ. 20 (1), 93–100. http://dx.doi.org/10.1046/j.1365-3040.1997.d01-16.x.

Göbel, L., Coners, H., Hertel, D., Willinghöfer, S., Leuschner, C., 2019. The role of low soil temperature for photosynthesis and stomatal conductance of three graminoids from different elevations. Front. Plant Sci. 10, 330. http://dx.doi.org/10.3389/fpls.2019.00330.

Grace, J., Lloyd, J., McIntyre, J., Miranda, A., Meir, P., Miranda, H., Moncrieff, J., Massheder, J., Wright, I., Gash, J., 1995. Fluxes of carbon dioxide and water vapour over an undisturbed tropical forest in south-west Amazonia. Global Change Biol. 1 (1), 1–12.

Griffiths, H., Cousins, A.B., Badger, M.R., von Caemmerer, S., 2007. Discrimination in the dark. Resolving the interplay between metabolic and physical constraints to phospho enol pyruvate carboxylase activity during the crassulacean acid metabolism cycle. Plant Physiol. 143 (2), 1055–1067. http://dx.doi.org/10.1104/pp.106.088302.

Heinemeyer, A., McNamara, N.P., 2011. Comparing the closed static versus the closed dynamic chamber flux methodology: Implications for soil respiration studies. Plant Soil 346 (1), 145–151. http://dx.doi.org/10.1007/s11104-011-0804-0.

Islam, T., Hossain, M.M., Covington, S., 2025. Natural fibers towards fashion sustainability: a review of raw materials, production, application, and perspective. J. Nat. Fibers 22 (1), 2462218. http://dx.doi.org/10.1080/15440478.2025.2462218.

Jardim, A.M.d.R.F., de Morais, J.E.F., de Souza, L.S.B., Marin, F.R., de Moura, M.S.B., Morellato, L.P.C., de Assunção Montenegro, A.A., Ometto, J.P.H.B., de Lima, J.L., Júnior, J.C.B.D., et al., 2023. Sink or carbon source? how the opuntia cactus agroecosystem interacts in the use of carbon, nutrients and radiation in the Brazilian semi-arid region. J. Hydrol. 625, 130121. http://dx.doi.org/10.1016/j.jhydrol.2023.130121.

Keenan, T.F., Hollinger, D.Y., Bohrer, G., Dragoni, D., Munger, J.W., Schmid, H.P., Richardson, A.D., 2013. Increase in forest water-use efficiency as atmospheric carbon dioxide concentrations rise. Nature 499 (7458), 324–327. http://dx.doi.org/10.1038/nature12291.

Kevrešan, S., Krstić, B., Popović, M., Kovačev, L., Pajević, S., Kandrač, J., Malenčić, đ., 1997. Biochemical changes in sugar beet lines in dependence on soil moisture. Biol. Plant. 40, 245–250.

Kitz, F., Spielmann, F.M., Hammerle, A., Kolle, O., Migliavacca, M., Moreno, G., Ibrom, A., Krasnov, D., Noe, S.M., Wohlfahrt, G., 2020. Soil COS exchange: A comparison of three European ecosystems. Glob. Biogeochem. Cycles 34 (4), e2019GB006202.

Kljun, N., Calanca, P., Rotach, M., Schmid, H.P., 2015. A simple two-dimensional parameterisation for flux footprint prediction (FFP). Geosci. Model. Dev. 8 (11), 3695–3713. http://dx.doi.org/10.5194/gmd-8-3695-2015.

Kohonen, K.M., Dewar, R., Tramontana, G., Mauranen, A., Kolari, P., Kooijmans, L.M., Papale, D., Vesala, T., Mammarella, I., 2022. Intercomparison of methods to estimate gross primary production based on CO_2 and COS flux measurements. Biogeosciences 19 (17), 4067–4088. http://dx.doi.org/10.5194/bg-19-4067-2022.

Kohonen, K.M., Kolari, P., Kooijmans, L., Chen, H., Seibt, U., Sun, W., Mammarella, I., 2020. Towards standardized processing of eddy covariance flux measurements of carbonyl sulfide. Atmos. Meas. Tech. 13 (7), 3957–3975. http://dx.doi.org/10.5194/amt-13-3957-2020.

Kooijmans, L.M., Cho, A., Ma, J., Kaushik, A., Haynes, K., Baker, I., Luijkx, I., Groenink, M., Peters, W., Miller, J.B., Berry, J.A., Ogée, J., Meredith, L.K., Sun, W., Kohonen, K.-M., Vesala, T., Mammarella, I., Chen, H., Spielmann, F.M., Wohlfahrt, G., Berkelhammer, M., Whelan, M.E., Maseyk, K., Seibt, U., Commane, R., Wehr, R., Krol, M., 2021. Evaluation of carbonyl sulfide biosphere exchange in the simple biosphere model (SiB4). Biogeosci. Discuss. 1–32.

Kooijmans, L.M., Sun, W., Aalto, J., Erkkilä, K.-M., Maseyk, K., Seibt, U., Vesala, T., Mammarella, I., Chen, H., 2019. Influences of light and humidity on carbonyl sulfide-based estimates of photosynthesis. Proc. Natl. Acad. Sci. 116 (7), 2470–2475.

Kooijmans, L.M., Uitslag, N.A., Zahniser, M.S., Nelson, D.D., Montzka, S.A., Chen, H., 2016. Continuous and high-precision atmospheric concentration measurements of COS, CO_2, CO and H_2O using a quantum cascade laser spectrometer (QCLS). Atmos. Meas. Tech. 9 (11), 5293–5314. http://dx.doi.org/10.5194/amt-9-5293-2016.

Korrensalo, A., Männistö, E., Alekseychik, P., Mammarella, I., Rinne, J., Vesala, T., Tuittila, E.S., 2018. Small spatial variability in methane emission measured from a wet patterned boreal bog. Biogeosciences 15 (6), 1749–1761. http://dx.doi.org/10.5194/bg-15-1749-2018.

Kozłowski, R.M., Mackiewicz-Talarczyk, M., Barriga-Bedoya, J., 2020. 20 - new emerging natural fibres and relevant sources of information. In: Kozłowski, R.M., Mackiewicz-Talarczyk, M. (Eds.), Handbook of Natural Fibres (Second Edition), second ed. In: Woodhead Publishing Series in Textiles, Woodhead Publishing, pp. 747–787. http://dx.doi.org/10.1016/B978-0-12-818398-4.00022-0.

Langford, B., Acton, W., Ammann, C., Valach, A., Nemitz, E., 2015. Eddy-covariance data with low signal-to-noise ratio: time-lag determination , uncertainties and limit of detection. Atmos. Meas. Tech. 8, 4197–4213. http://dx.doi.org/10.5194/amt-8-4197-2015.

Lasslop, G., Reichstein, M., Papale, D., Richardson, A., Arneth, A., Barr, A., Stoy, P., Wohlfahrt, G., 2010. Separation of net ecosystem exchange into assimilation and respiration using a light response curve approach: critical issues and global evaluation. Global Change Biol. 16 (1), 187–208.

Lüttge, U., 2004. Ecophysiology of crassulacean acid metabolism (CAM). Ann. Botany 93 (6), 629–652. http://dx.doi.org/10.1093/aob/mch087.

Maignan, F., Abadie, C., Remaud, M., Kooijmans, L.M.J., Kohonen, K.-M., Commane, R., Wehr, R., Campbell, J.E., Belviso, S., Montzka, S.A., Raoult, N., Seibt, U., Shiga, Y.P., Vuichard, N., Whelan, M.E., Peylin, P., 2021. Carbonyl sulfide: comparing a mechanistic representation of the vegetation uptake in a land surface model and the leaf relative uptake approach. Biogeosciences 18 (9), 2917–2955. http://dx.doi.org/10.5194/bg-18-2917-2021.

Mammarella, I., Peltola, O., Nordbo, A., Järvi, L., Rannik, Ü., 2016. Quantifying the uncertainty of eddy covariance fluxes due to the use of different software packages and combinations of processing steps in two contrasting ecosystems. Atmos. Meas. Tech. 9 (10), 4915–4933. http://dx.doi.org/10.5194/amt-9-4915-2016.

Maseyk, K., Berry, J.A., Billesbach, D., Campbell, J.E., Torn, M.S., Zahniser, M., Seibt, U., 2014. Sources and sinks of carbonyl sulfide in an agricultural field in the southern great plains. Proc. Natl. Acad. Sci. 111 (25), 9064–9069. http://dx.doi.org/10.1073/pnas.1319132111.

Monteith, J., 1965. Evaporation and environment. Symp. Soc. Exp. Biol. 19, 205–234.

Nobel, P., 1996. High productivity of certain agronomic CAM species. In: Winter, K., Smith, J.A.C. (Eds.), Crassulacean Acid Metabolism: Biochemistry, Ecophysiology and Evolution. Springer, pp. 255–265.

Nobel, P., Valenzuela, A., 1987. Environmental responses and productivity of the CAM plant, agave tequilana. Agricult. Forest. Meterol. 39 (4), 319–334. http://dx.doi.org/10.1016/0168-1923(87)90024-4.

Osmond, C., 1978. Crassulacean acid metabolism: a curiosity in context. Annu. Rev. Plant Physiol. 29 (1), 379–414. http://dx.doi.org/10.1146/annurev.pp.29.060178.002115.

Owen, N.A., Choncubhair, Ó.N., Males, J., del Real Laborde, J.I., Rubio-Cortés, R., Griffiths, H., Lanigan, G., 2016. Eddy covariance captures four-phase crassulacean acid metabolism (CAM) gas exchange signature in agave. Plant Cell Environ. 39 (2), 295–309. http://dx.doi.org/10.1111/pce.12610.

Pellikka, P., Luotamo, M., Sädekoski, N., Hietanen, J., Vuorinne, I., Räsänen, M., Heiskanen, J., Siljander, M., Karhu, K., Klami, A., 2023. Tropical altitudinal gradient soil organic carbon and nitrogen estimation using specim IQ portable imaging spectrometer. Sci. Total Environ. 883 (16367).

Protoschill-Krebs, G., Kesselmeier, J., 1992. Enzymatic pathways for the consumption of carbonyl sulphide (COS) by higher plants. Bot. Acta 105 (3), 206–212.

Rannik, Ü., 1998. On the surface layer similarity at a complex forest site. J. Geophys. Res.: Atmos. 103 (D8), 8685–8697.

Reichstein, M., Falge, E., Baldocchi, D., Papale, D., Aubinet, M., Berbigier, P., Bernhofer, C., Buchmann, N., Gilmanov, T., Granier, A., Grünwald, T., Havránková, K., Ilvesniemi, H., Janous, D., Knohl, A., Laurila, T., Lohila, A., Loustau, D., Matteucci, G., Meyers, T., Miglietta, F., Ourcival, J.M., Pumpanen, J., Rambal, S., Rotenberg, E., Sanz, M., Tenhunen, J., Seufert, G., Vaccari, F., Vesala, T., Yakir, D., Valentini, R., 2005. On the separation of net ecosystem exchange into assimilation and ecosystem respiration: Review and improved algorithm. Global Change Biol. 11 (9), 1424–1439. http://dx.doi.org/10.1111/j.1365-2486.2005.001002.x.

San-José, J., Montes, R., Nikonova, N., 2007. Diurnal patterns of carbon dioxide, water vapour, and energy fluxes in pineapple [Ananas comosus (L.) Merr. cv. Red Spanish] field using eddy covariance. Photosynthetica 45, 370–384.

Sandoval-Soto, L., Stanimirov, M., Von Hobe, M., Schmitt, V., Valdes, J., Wild, A., Kesselmeier, J., 2005. Global uptake of carbonyl sulfide (COS) by terrestrial vegetation: Estimates corrected by deposition velocities normalized to the uptake of carbon dioxide (CO_2). Biogeosciences 2, 125–132.

Schulze, E., Beck, E., Buchmann, N., Clemens, S., Müller-Hohenstein, K., Scherer-Lorenzen, M., 2019. Plant Ecology, second ed. Springer, p. 928.

Seibt, U., Kesselmeier, J., Sandoval-Soto, L., Kuhn, U., Berry, J.A., 2010. A kinetic analysis of leaf uptake of COS and its relation to transpiration, photosynthesis and carbon isotope fractionation. Biogeosciences 7 (1), 333–341. http://dx.doi.org/10.5194/bg-7-333-2010.

Shapley, L.S., 1953. Stochastic games. Proc. Natl. Acad. Sci. 39 (10), 1095–1100. http://dx.doi.org/10.1073/pnas.39.10.1095.

Skogberg, M., Kohonen, K.M., Lohila, A., Merbold, L., Räsänen, M., Vuorinne, I., Pellikka, P., Vesala, T., Kübert, A., 2025. Ecosystem-scale crassulacean acid metabolism (CAM) gas exchange of a sisal (agave sisalana) plantation. Agric. Ecosyst. Environ. 381 (109435), http://dx.doi.org/10.1016/j.agee.2024.109435.

Spielmann, F.M., Hammerle, A., Kitz, F., Gerdel, K., Wohlfahrt, G., 2020. Seasonal dynamics of the COS and CO_2 exchange of a managed temperate grassland. Biogeosciences 17 (16), 4281–4295. http://dx.doi.org/10.5194/bg-17-4281-2020.

Spielmann, F., Wohlfahrt, G., Hammerle, A., Kitz, F., Migliavacca, M., Alberti, G., Ibrom, A., El-Madany, T.S., Gerdel, K., Moreno, G., Kolle, O., Karl, T., Peressotti, A., Delle Vedove, G., 2019. Gross primary productivity of four European ecosystems constrained by joint CO_2 and COS flux measurements. Geophys. Res. Lett. 46 (10), 5284–5293.

Stimler, K., Montzka, S.A., Berry, J.A., Rudich, Y., Yakir, D., 2010. Relationships between carbonyl sulfide (COS) and CO_2 during leaf gas exchange. New Phytol. 186 (4), 869–878.

Stoy, P.C., El-Madany, T.S., Fisher, J.B., Gentine, P., Gerken, T., Good, S.P., Klosterhalfen, A., Liu, S., Miralles, D.G., Perez-Priego, O., et al., 2019. Reviews and syntheses: Turning the challenges of partitioning ecosystem evaporation and transpiration into opportunities. Biogeosciences 16 (19), 3747–3775. http://dx.doi.org/10.5194/bg-16-3747-2019.

Sun, W., Maseyk, K., Lett, C., Seibt, U., 2018. Stomatal control of leaf fluxes of carbonyl sulfide and CO_2 in a typha freshwater marsh. Biogeosciences 15 (11), 3277–3291.

Sun, W., Maseyk, K., Lett, C., Seibt, U., 2024. Restricted internal diffusion weakens transpiration–photosynthesis coupling during heatwaves: Evidence from leaf carbonyl sulphide exchange. Plant Cell Environ. 47 (5), 1813–1833. http://dx.doi.org/10.1111/pce.14840.

Vesala, T., Kohonen, K.-M., Kooijmans, L., Praplan, A., Foltýnová, L., Kolari, P., Kulmala, M., Bäck, J., Nelson, D., Yakir, D., Zahniser, M., Mammarella, I., 2022. Long-term fluxes of carbonyl sulfide and their seasonality and interannual variability in a boreal forest. Atmos. Chem. Phys. 22 (4), 2569–2584. http://dx.doi.org/10.5194/acp-22-2569-2022.

Vesala, T., Suni, T., Rannik, Ü., Keronen, P., Markkanen, T., Sevanto, S., Grönholm, T., Smolander, S., Kulmala, M., Ilvesniemi, H., et al., 2005. Effect of thinning on surface fluxes in a boreal forest. Glob. Biogeochem. Cycles 19 (2).

Vuorinne, I., Heiskanen, J., Maghenda, M., Mwangala, L., Muukkonen, P., Pellikka, P., 2021a. Allometric models for estimating leaf biomass of sisal in a semi-arid environment in Kenya. Biomass Bioenergy 155 (106294).

Vuorinne, I., Heiskanen, J., Pellikka, P., 2021b. Assessing leaf biomass of agave sisalana using sentinel-2 vegetation indices. Remote. Sens. 13 (233), http://dx.doi.org/10.3390/rs13020233.

Wachiye, S., Merbold, L., Vesala, T., Rinne, J., Leitner, S., Räsänen, M., Vuorinne, I., Heiskanen, J., Pellikka, P., 2021. Soil greenhouse gas emissions from a sisal chronosequence in Kenya. Agricult. Forest. Meterol. 307, http://dx.doi.org/10.1016/j.agrformet.2021.108465.

Wehr, R., Commane, R., Munger, J.W., McManus, J.B., Nelson, D.D., Zahniser, M.S., Saleska, S.R., Wofsy, S.C., 2017. Dynamics of canopy stomatal conductance, transpiration, and evaporation in a temperate deciduous forest, validated by carbonyl sulfide uptake. Biogeosciences 14, 389–401. http://dx.doi.org/10.5194/bg-2016-365.

Wehr, R., Saleska, S.R., 2021. Calculating canopy stomatal conductance from eddy covariance measurements, in light of the energy budget closure problem. Biogeosciences 18 (1), 13–24. http://dx.doi.org/10.5194/bg-18-13-2021.

Winter, K., 2019. Ecophysiology of constitutive and facultative CAM photosynthesis. J. Exp. Bot. 70 (22), 6495–6508. http://dx.doi.org/10.1093/jxb/erz002.

Winter, K., Smith, J., 1996. An introduction to crassulacean acid metabolism. Biochemical principles and ecological diversity. In: Crassulacean Acid Metabolism: Biochemistry, Ecophysiology and Evolution. Springer, pp. 1–13.

Winter, K., Smith, J.A.C., 2022. CAM photosynthesis: the acid test. New Phytol. 233 (2), 599–609. http://dx.doi.org/10.1111/nph.17790.

Wohlfahrt, G., Brilli, F., Hörtnagl, L., Xu, X., Bingemer, H., Hansel, A., Loreto, F., 2012. Carbonyl sulfide (COS) as a tracer for canopy photosynthesis, transpiration and stomatal conductance: potential and limitations. Plant Cell Environ. 35 (4), 657–667.

Wohlfahrt, G., Gerdel, K., Migliavacca, M., Rotenberg, E., Tatarinov, F., Müller, J., Hammerle, A., Julitta, T., Spielmann, F., Yakir, D., 2018. Sun-induced fluorescence and gross primary productivity during a heat wave. Sci. Rep. 8 (1), 1–9.

Yang, X., Cushman, J.C., Borland, A.M., Edwards, E.J., Wullschleger, S.D., Tuskan, G.A., Owen, N.A., Griffiths, H., Smith, J.A.C., De Paoli, H.C., Weston, D.J., Cottingham, R., Hartwell, J., Davis, S.C., Silvera, K., Ming, R., Schlauch, K., Abraham, P., Stewart, J.R., Guo, H.-B., Albion, R., Ha, J., Lim, S.D., Wone, B.W.M., Yim, W.C., Garcia, T., Mayer, J.A., Petereit, J., Nair, S.S., Casey, E., Hettich, R.L., Ceusters, J., Ranjan, P., Palla, K.J., Yin, H., Reyes-García, C., Andrade, J.L., Freschi, L., Beltrán, J.D., Dever, L.V., Boxall, S.F., Waller, J., Davies, J., Bupphada, P., Kadu, N., Winter, K., Sage, R.F., Aguilar, C.N., Schmutz, J., Jenkins, J., Holtum, J.A.M., 2015. A roadmap for research on crassulacean acid metabolism (CAM) to enhance sustainable food and bioenergy production in a hotter, drier world. New Phytol. 207 (3), 491–504. http://dx.doi.org/10.1111/nph.13393.

Yang, X., Liu, Y., Yuan, G., Weston, D.J., Tuskan, G.A., 2024. Engineering crassulacean acid metabolism in c_3 and c_4 plants. Cold Spring Harb. Perspect. Biol. 16 (4), a041674. http://dx.doi.org/10.1101/cshperspect.a041674.

Yang, F., Qubaja, R., Tatarinov, F., Rotenberg, E., Yakir, D., 2018. Assessing canopy performance using carbonyl sulfide measurements. Global Change Biol. 24 (8), 3486–3498. http://dx.doi.org/10.1111/gcb.14145.

Zahn, E., Bou-Zeid, E., Good, S.P., Katul, G.G., Thomas, C.K., Ghannam, K., Smith, J.A., Chamecki, M., Dias, N.L., Fuentes, J.D., Alfieri, J.G., Kwon, H., Caylor, K.K., Gao, Z., Soderberg, K., Bambach, N.E., Hipps, L.E., Prueger, J.H., Kustas, W.P., 2022. Direct partitioning of eddy-covariance water and carbon dioxide fluxes into ground and plant components. Agricult. Forest. Meterol. 315, 108790. http://dx.doi.org/10.1016/j.agrformet.2021.108790.